Numerical Simulation of Compressible Flow in an Asymmetric Vocal Jet

Petr Šimánek and Miloslav Feistauer

***Abstract*—The paper is concerned with numerical simulation of a compressible flow in time-dependent asymmetric 2D and 3D vocal jets. The mathematical model of this process is described by the compressible Navier-Stokes equations. For the treatment of the time-dependent domain, the arbitrary Lagrangian-Eulerian (ALE) method is used. The discontinuous Galerkin finite element method (DGFEM) is applied to the space semidiscretization of the governing equations in the ALE formulation. The time discretization is carried out with the aid of a linearized semi-implicit backward Euler method with good stability properties. We present some computational results for the flow in a channel, representing a model of glottis and a part of the vocal tract, with a prescribed motion of the channel walls at the position of vocal folds.**

***Index Terms*—vocal jet, compressible Navier-Stokes equations, ALE formulation, discontinuous Galerkin method, fluid-structure interaction.**

I. Introduction

THIS paper is concerned with the numerical simulation of compressible flow in 2D and 3D channels with moving walls. The goal is to work out the method allowing the analysis of flow-induced oscillatory motion of the vocal folds during human phonation, which leads to a pulsating jet-like flow penetrating into the cavity downstream of the glottis.

The knowledge of the glottal flow is important for the understanding of the processes of the voice production and also in the development of voice protheses (cf. e.g., [12]). In [1] we can find an overview of the current state of mathematical models for the human phonation process. Such models are valuable tools for providing insight into the basic mechanisms of phonation and in future could help with surgical planning, diagnostics and voice rehabilitation. In current publications various simplified glottal flow models are used. They are based on the Bernoulli equation (cf. [13]), 1D models for an incompressible inviscid fluid (cf. [7]), 2D incompressible Navier-Stokes equations solved by the finite volume method (cf. [2]) or finite element method (cf. [15]). Acoustic wave propagation in the vocal tract is usually modeled separately using linear acoustic perturbation theory (cf. [14]). The paper [11] is devoted to the 3D finite element simulation of vibrating human vocal folds.

Manuscript received July 1, 2013; revised July 13, 2013. This work was supported by the grant No. 549912 of the Grant Agency of the Charles University in Prague (P. Šimánek) and the grant No. 13-00522S of the Czech Science Foundation (M. Feistauer).

P. Šimánek is with the Charles University in Prague, Faculty of Mathematics and Physics, Sokolovská 83, 18675 Praha 8, Czech Republic, e-mail: psimanek@atlas.cz.

M. Feistauer is with the Charles University in Prague, Faculty of Mathematics and Physics, Sokolovská 83, 18675 Praha 8, Czech Republic, e-mail: feist@karlin.mff.cuni.cz

Most of models of flow through vocal folds are based on the incompressible Navier-Stokes equations. Here we shall be concerned with the model of compressible flow. The system of the compressible Navier-Stokes equations written in the ALE (arbitrary Lagrangian-Eulerian) form is discretized in space by the discontinuous Galerkin (DG) finite element method using piecewise polynomial approximations without the requirement of the continuity of the approximate solution on interfaces between neighboring elements. This method appears to be robust with respect to the magnitude of the Mach number and the Reynolds number. See, e.g., [5], [4].

A. ALE Navier-Stokes problem

We are concerned with the numerical solution of compressible flow in a domain $\Omega_t \subset I\!R^3$ depending on time $t \in [0,T]$. Let the boundary of Ω_t consist of three different disjoint parts - $\partial\Omega_t = \Gamma_I \cup \Gamma_O \cup \Gamma_{W_t}$, where Γ_I is the inlet, Γ_O is the outlet and Γ_{W_t} is the moving impermeable boundary of the vocal folds.

The time dependence of the domain is taken into account with the aid of a one-to-one ALE mapping (cf. [3]) $\mathcal{A}_t : \Omega_0 \longrightarrow \Omega_t$, i.e. $\mathcal{A}_t : X \longmapsto x = x(X,t) = \mathcal{A}_t(X)$. We define the domain velocity $\tilde{z}(X,t) = \partial\mathcal{A}_t(X)/\partial t$, $z(x,t) = \tilde{z}(\mathcal{A}^{-1}(x),t)$, $t \in [0,T]$, $X \in \Omega_0$, $x \in \Omega_t$, and the ALE derivative of a function $f = f(x,t)$ defined for $x \in \Omega_t$ and $t \in (0,T)$: $D^A f(x,t)/Dt = \partial\tilde{f}(X,t)/\partial t$, where $\tilde{f}(X,t) = f(\mathcal{A}_t(X),t)$, $X \in \Omega_0$.

We write the system describing compressible flow (consisting of the continuity equation, the Navier-Stokes equations and the energy equation) in the ALE form

$$\frac{D^A \boldsymbol{w}}{Dt} + \sum_{s=1}^{3} \frac{\partial \boldsymbol{g}_s(\boldsymbol{w})}{\partial x_s} + \boldsymbol{w}\,\mathrm{div}\boldsymbol{z} = \sum_{s=1}^{3} \frac{\partial \boldsymbol{R}_s(\boldsymbol{w},\nabla\boldsymbol{w})}{\partial x_s}, \quad (1)$$

where

$$\begin{aligned}
\boldsymbol{w} &= (w_1,\dots,w_5)^T \\
&= (\rho,\rho v_1,\rho v_2,\rho v_3,E)^T \in I\!R^5, \\
\boldsymbol{g}_i(\boldsymbol{w}) &= \boldsymbol{f}_i(\boldsymbol{w}) - z_i\boldsymbol{w}, \\
\boldsymbol{f}_i(\boldsymbol{w}) &= (f_{i1},\cdots,f_{i5})^T \\
&= (\rho v_i, \rho v_1 v_i + \delta_{1i}\,p, \rho v_2 v_i + \delta_{2i}\,p, \\
&\quad \rho v_3 v_i + \delta_{3i}\,p, (E+p)v_i)^T, \\
\boldsymbol{R}_i(\boldsymbol{w},\nabla\boldsymbol{w}) &= (R_{i1},\dots,R_{i5})^T \\
&= (0,\tau_{i1}^V,\tau_{i2}^V,\tau_{i3}^V, \\
&\quad \tau_{i1}^V v_1 + \tau_{i2}^V\,v_2 + \tau_{i3}^V v_3 + k\partial\theta/\partial x_i)^T, \\
\tau_{ij}^V &= \lambda\,\mathrm{div}\boldsymbol{v}\,\delta_{ij} + 2\mu\,d_{ij}(\boldsymbol{v}), \\
d_{ij}(\boldsymbol{v}) &= (\partial v_i/\partial x_j + \partial v_j/\partial x_i)/2.
\end{aligned}$$

ISBN: 978-988-19253-1-2
ISSN: 2078-0958 (Print); ISSN: 2078-0966 (Online)

The following notation is used: p - pressure (Pa), ρ - fluid density (kg/m^3), $\boldsymbol{v} = (v_1, v_2, v_3)$ - velocity (m/s), E - total energy (J), θ - absolute temperature (K), $\gamma > 1$ - Poisson adiabatic constant, $c_v > 0$ - specific heat at constant volume, $\mu > 0, \lambda = -2\mu/3$ - viscosity coefficients, k - heat conduction. The vector-valued function $\boldsymbol{w}$ is called the state vector, the functions $\boldsymbol{f}_i$ are the inviscid fluxes and $\boldsymbol{R}_i$ are viscous terms.

System (1) is completed by the thermodynamical relations:

$$p = (\gamma - 1)(E - \rho|\boldsymbol{v}|^2/2), \quad \theta = \left(E/\rho - |\boldsymbol{v}|^2/2\right)/c_v.$$

We consider the initial condition $\boldsymbol{w}(x,0) = \boldsymbol{w}^0(x)$, $x \in \Omega_0$, and the boundary conditions: $\rho = \rho_D$, $\boldsymbol{v} = \boldsymbol{v}_D$, $\sum_{i,j=1}^3 \tau_{ij}^V n_i v_j + k\frac{\partial\theta}{\partial n} = 0$ on Γ_I, $\boldsymbol{v}|_{\Gamma_{W_t}} = \boldsymbol{z}_D$ - velocity of a moving wall, $\partial\theta/\partial n = 0$ on Γ_{W_t}, $\sum_{i=1}^3 \tau_{ij}^V n_i = 0$, $j = 1, 2, 3$, $\partial\theta/\partial n = 0$ on Γ_O, with given data $\boldsymbol{w}^0$, ρ_D, $\boldsymbol{v}_D$, $\boldsymbol{z}_D$.

The whole problem can easily be modified in the 2D case.

B. Discretization

We use the discontinuous Galerkin finite element method for the space semidiscretization of the Navier-Stokes system (1). We consider a polygonal approximation Ω_{ht} of the domain Ω_t. By $\mathcal{T}_{ht}$ we denote a partition of the closure $\overline{\Omega}_{ht}$ into a finite number of tetrahedra (in 3D) or triangles (in 2D) K with disjoint interiors. By $\mathcal{F}_{ht}$ we denote the system of all faces of all elements $K \in \mathcal{T}_{ht}$. Further, we introduce the set of all interior faces $\mathcal{F}_{ht}^I$, the set of all boundary faces $\mathcal{F}_{ht}^B$ and the set of all Dirichlet boundary faces $\mathcal{F}_{ht}^D$, on which Dirichlet conditions are prescribed. Each $\Gamma \in \mathcal{F}_{ht}$ is associated with a unit normal vector $\boldsymbol{n}_\Gamma$ to Γ. For $\Gamma \in \mathcal{F}_{ht}^B$ the normal $\boldsymbol{n}_\Gamma$ has the same orientation as the outer normal to $\partial\Omega_{ht}$. For each $\Gamma \in \mathcal{F}_{ht}^I$ there exist two neighbouring elements $K_\Gamma^{(L)}, K_\Gamma^{(R)} \in \mathcal{T}_h$ such that $\Gamma \subset \partial K_\Gamma^{(R)} \cap \partial K_\Gamma^{(L)}$. We use the convention that $K_\Gamma^{(R)}$ lies in the direction of $\boldsymbol{n}_\Gamma$ and $K_\Gamma^{(L)}$ lies in the opposite direction to $\boldsymbol{n}_\Gamma$. If $\Gamma \in \mathcal{F}_{ht}^B$, then the element adjacent to Γ will be denoted by $K_\Gamma^{(L)}$. By $d = 2$ or 3 we denote the dimension of the problem. The approximate solution will be sought in the space of discontinuous piecewise polynomial functions $\boldsymbol{S}_{ht} = [S_{ht}]^{d+2}$, with $S_{ht} = \{v; v|_K \in P_r(K)\ \forall K \in \mathcal{T}_{ht}\}$, where $r > 0$ is an integer and $P_r(K)$ denotes the space of all polynomials on K of degree $\le r$. A function $\boldsymbol{\varphi} \in \boldsymbol{S}_{ht}$ is, in general, discontinuous on interfaces $\Gamma \in \mathcal{F}_{ht}^I$. By $\boldsymbol{\varphi}_\Gamma^{(L)}$ and $\boldsymbol{\varphi}_\Gamma^{(R)}$ we denote the values of $\boldsymbol{\varphi}$ on Γ considered from the interior and the exterior of $K_\Gamma^{(L)}$, respectively, and set $\langle\boldsymbol{\varphi}\rangle_\Gamma = (\boldsymbol{\varphi}_\Gamma^{(L)} + \boldsymbol{\varphi}_\Gamma^{(R)})/2$, $[\boldsymbol{\varphi}]_\Gamma = \boldsymbol{\varphi}_\Gamma^{(L)} - \boldsymbol{\varphi}_\Gamma^{(R)}$. By $d(\Gamma)$ we denote the diameter of Γ.

For the time discretization we construct a partition $0 = t_0 < t_1 < t_2 \ldots$ of the time interval $[0, T]$ and define the time step $\tau_k = t_{k+1} - t_k$. We use the approximations $\boldsymbol{w}_h(t_n) \approx \boldsymbol{w}_h^n \in \boldsymbol{S}_{ht_n}$, $\boldsymbol{z}(t_n) \approx \boldsymbol{z}^n$, $n = 0, 1, \ldots$, and introduce the function $\hat{\boldsymbol{w}}_h^k = \boldsymbol{w}_h^k \circ \mathcal{A}_{t_k} \circ \mathcal{A}_{t_{k+1}}^{-1}$, which is defined in the domain $\Omega_{ht_{k+1}}$.

The resulting scheme is the following: For $k = 0, 1, \ldots$, find $\boldsymbol{w}_h^{k+1} \in \boldsymbol{S}_{ht_{k+1}}$ such that

$$\begin{aligned}
&\left(\frac{\boldsymbol{w}_h^{k+1} - \hat{\boldsymbol{w}}_h^k}{\tau_k}, \boldsymbol{\varphi}_h\right) \\
&+\hat{b}_h(\hat{\boldsymbol{w}}_h^k, \boldsymbol{w}_h^{k+1}, \boldsymbol{\varphi}_h) \\
&+\hat{a}_h(\hat{\boldsymbol{w}}_h^k, \boldsymbol{w}_h^{k+1}, \boldsymbol{\varphi}_h) \\
&+J_h(\boldsymbol{w}_h^{k+1}, \boldsymbol{\varphi}_h) + d_h\left(\boldsymbol{w}_h^{k+1}, \boldsymbol{\varphi}_h\right) \\
&+\hat{\beta}_h(\boldsymbol{w}_h^k, \boldsymbol{w}_h^{k+1}, \boldsymbol{\varphi}_h) + \hat{J}_h(\boldsymbol{w}_h^k, \boldsymbol{w}_h^{k+1}, \boldsymbol{\varphi}_h) \\
&= \ell(\boldsymbol{w}_B^k, \boldsymbol{\varphi}), \qquad \forall \boldsymbol{\varphi}_h \in \boldsymbol{S}_{ht_{k+1}}.
\end{aligned} \tag{2}$$

The forms in (2) are defined on the basis of the properties of the inviscid and viscous terms in system (1). We have

$$\begin{aligned}
&\hat{b}_h(\hat{\boldsymbol{w}}_h^k, \boldsymbol{w}_h^{k+1}, \boldsymbol{\varphi}_h) = \\
&-\sum_{K\in\mathcal{T}_{ht_{k+1}}} \int_K \sum_{s=1}^d (\mathbf{A}_s(\hat{\boldsymbol{w}}_h^k(x)) \\
&-z_s^{k+1}(x))\mathbf{I})\boldsymbol{w}_h^{k+1}(x)) \cdot \frac{\partial\boldsymbol{\varphi}_h(x)}{\partial x_s}\,dx \\
&+\sum_{\Gamma\in\mathcal{F}_{ht_{k+1}}^I} \int_\Gamma \Big(\mathbf{P}_g^+\left(\langle\hat{\boldsymbol{w}}_h^k\rangle_\Gamma, \boldsymbol{n}_\Gamma\right)\boldsymbol{w}_{h\Gamma}^{k+1(L)} \\
&+\mathbf{P}_g^-\left(\langle\hat{\boldsymbol{w}}_h^k\rangle_\Gamma, \boldsymbol{n}_\Gamma\right)\boldsymbol{w}_{h\Gamma}^{k+1(R)}\Big) \cdot [\boldsymbol{\varphi}_h]_\Gamma\,dS \\
&+\sum_{\Gamma\in\mathcal{F}_{ht_{k+1}}^B} \int_\Gamma \Big(\mathbf{P}_g^+\left(\langle\hat{\boldsymbol{w}}_h^k\rangle_\Gamma, \boldsymbol{n}_\Gamma\right)\boldsymbol{w}_{h\Gamma}^{k+1(L)} \\
&+\mathbf{P}_g^-\left(\langle\hat{\boldsymbol{w}}_h^k\rangle_\Gamma, \boldsymbol{n}_\Gamma\right)\hat{\boldsymbol{w}}_{h\Gamma}^{k(R)}\Big) \cdot \boldsymbol{\varphi}_h\,dS,
\end{aligned}$$

$$\begin{aligned}
&\hat{a}_h(\hat{\boldsymbol{w}}_h^k, \boldsymbol{w}_h^{k+1}, \boldsymbol{\varphi}_h) = \\
&\sum_{K\in\mathcal{T}_{ht_{k+1}}} \int_K \sum_{s=1}^d \mathbf{R}_s(\hat{\boldsymbol{w}}_h^k, \nabla\boldsymbol{w}_h^{k+1}) \cdot \frac{\partial\boldsymbol{\varphi}_h}{\partial x_s}\,dx \\
&-\sum_{\Gamma\in\mathcal{F}_{ht_{k+1}}^I} \int_\Gamma \sum_{s=1}^d \left\langle\mathbf{R}_s(\hat{\boldsymbol{w}}_h^k, \nabla\boldsymbol{w}^{k+1})\right\rangle(\boldsymbol{n}_\Gamma)_s \cdot [\boldsymbol{\varphi}_h]_\Gamma\,dS \\
&-\sum_{\Gamma\in\mathcal{F}_{ht_{k+1}}^D} \int_\Gamma \sum_{s=1}^d \mathbf{R}_s(\hat{\boldsymbol{w}}_h^k, \nabla\boldsymbol{w}_h^{k+1})(\boldsymbol{n}_\Gamma)_s \cdot \boldsymbol{\varphi}_h\,dS,
\end{aligned}$$

$$\begin{aligned}
&J_h(\boldsymbol{w}, \boldsymbol{\varphi}_h) = \sum_{\Gamma\in\mathcal{F}_{ht}^I} \int_\Gamma \sigma[\boldsymbol{w}]_\Gamma \cdot [\boldsymbol{\varphi}_h]_\Gamma\,dS \\
&+\sum_{\Gamma\in\mathcal{F}_{ht}^D} \int_\Gamma \sigma\boldsymbol{w} \cdot \boldsymbol{\varphi}_{h\Gamma}^{(L)}\,dS,
\end{aligned}$$

$$d_h(\boldsymbol{w}, \boldsymbol{\varphi}_h) = \sum_{K\in\mathcal{T}_{ht}} \int_K (\boldsymbol{w} \cdot \boldsymbol{\varphi}_h)\,\mathrm{div}\boldsymbol{z}\,dx,$$

$$\ell_h(\boldsymbol{w}, \boldsymbol{\varphi}_h) = \sum_{\Gamma\in\mathcal{F}_{ht}^D} \int_\Gamma \sum_{s=1}^d \sigma\boldsymbol{w}_B \cdot \boldsymbol{\varphi}_{h\Gamma}^{(L)}\,dS.$$

$\mathbf{A}_s(\boldsymbol{w})$ is the Jacobi matrix of the flux $\boldsymbol{f}_s(\boldsymbol{w})$, $\mathbf{P}_{\mathbf{g}}^{\pm}(\boldsymbol{w}, \boldsymbol{n})$ denotes the positive and negative parts of the Jacobi matrix of the flux $\sum_{s=1}^d \boldsymbol{g}_s(\boldsymbol{w})n_s$ (see [3]) and $\sigma|_\Gamma = C_W\mu/d(\Gamma)$, where $C_W > 0$ is a sufficiently large constant. The boundary state $\boldsymbol{w}_B$ is defined on the basis of extrapolation and the Dirichlet conditions. The determination of the state $\hat{\boldsymbol{w}}_h^{k(R)_\Gamma}$

ISBN: 978-988-19253-1-2
ISSN: 2078-0958 (Print); ISSN: 2078-0966 (Online)

Fig. 1. Vocal chord model in $0\,^\circ$ state.

is based on a linearized initial-boundary value Riemann problem described in [3].

Resulting system of linear equations was solved by GMRES method from PETSC [8] package.

The computation of the ALE mapping and the mesh motion are based on an artificial stationary elasticity problem treated similarly as in [6].

C. CFD model of vocal chords

Simplified model of glottis often used in literature and experiments (see e.g., [16], [11]) is M5 glottal model (Fig. 1) (detailed model description can be found in [10]). A quadrangular 3D channel of length of 6 cm and width and depth of 1.2 cm is employed, with glottal folds beginning 0.3 cm downstream to the inlet. This model can be easily adapted to different glottal angles from diverging (Fig. 2(a), $-40\,^\circ$) to converging (Fig. 2(b), $40\,^\circ$) shape. In computations in [16] the pulsation of glottal jet was produced by vertical vibration of vocal chords with fixed glottal divergence angle. In this work pulsation was produced by divergent-convergent shape change, angle ranged from $-40\,^\circ$ to $40\,^\circ$, vibration frequency was set to 100 Hz (i.e. time of one cycle is $T = 0.01$ s). This motion does not involve absolute closure of vocal folds, minimal clearance is 0.03 cm. Smaller clearance was not possible due to mesh distortion. To mimic the effect of the closure inlet velocity was reduced to 0 for 10% of the cycle when reaching the clearance minimum i.e. diverging shape of glottis with angle $-40\,^\circ$. This corresponds to time 0.2T-0.3T. Cases with reduced inlet velocity are denoted as "RIV". Cases with non-zero leakage during the whole phonation cycle can occur in pathological laryngeal flow (e.g., with vocal polyp).

Results were computed with $Re = \sqrt{\Delta P/\rho} h_{max}/\nu = 1225$ [16] based on the maximum vocal fold clearance $h_{max} = 0.1$cm and the pressure drop $\Delta P = 1$kPa, ρ and ν are the density and kinematic viscosity.

Computational meshes consisting of tetrahedral or triangular elements were created in GMSH ([9]). In the current study we used 191052 tetrahedral elements in 3D case and 21352 triangular elements in 2D case. Test functions of quadratic polynomials were used. The time step was set to 10^{-7}s. Mesh resolution was subject to refinement study (254032 tetrahedral, 43021 triangular elements), only in the case with static boundaries and we observed only minor changes (these results are not presented here). Model validation will be carried out by the comparison with experiments that are in preparation in the Institute of Thermomechanics of the Czech Academy of Sciences in Prague.

D. Results and discussion

The deflection of the glottal jet is usually found with divergent shape (Fig. 2(a)), which is why only the divergent shape was studied in [16], where authors propose hypothesis that the dominant effect for the asymmetric glottal jet deflection is the interaction of the jet with remnant vortices in postglottal region.

We present results of two 2D and two 3D computations. We show velocity magnitude at ten different time instants - $0.002s$, $0.004s$, $0.006s$, $0.008s$, $0.01s$, $0.012s$, $0.014s$, $0.016s$, $0.018s$ and $0.02s$ during first two cycles of movement. In Fig. 3 velocity magnitude contours in the 2D case without the reduced inlet velocity (RIV) (Fig. 3(a)) and with RIV (Fig. 3(b)) are compared. We can observe that the largest deflection occurs with the smallest clearance (divergent shape), where the jet velocity is comparable with velocity of the postglottal flow and that the deflection is smaller with convergent shape. Different jet deflection behaviour between cases with RIV and without RIV can be the result of weaker vortices in the postglottal region in the case with RIV. Y-coordinate of a point with the highest velocity 0.003 cm downstream the glottal folds in six phonation cycles is presented in Fig. 9. The 2D case without RIV shows substantially different jet deflection behaviour than the line representing the 2D case with RIV. Vorticity contours in Figs. 5 show different vortical structures in the case without RIV (Fig. 5(a)) and RIV (Fig. 5(b)). These findings seem to be in line with [16].

We furthermore present two 3D cases in Figs. 4, the case without RIV (Fig. 4(a)) and the case with RIV (Fig. 4(b)). The vorticity in Figs. 6 (Fig. 6(a) shows the case without RIV and Fig. 6(b) shows the situation with RIV) displays much weaker vortices than in the 2D case, which could (according to [16]) imply smaller asymmetrical jet deflection. However, as can be inspected in Fig. 9 or Fig. 10, the deflection angles are not significantly different from 2D cases. The 2D and 3D cases with RIV show very similar behaviour. The big peaks on 3D with RIV line occur in the moment of RIV.

The presence of RIV seems to have effect on some vortical structures in postglottal region as can be seen in Figs. 7 (case without RIV (Fig. 7(a)), case with RIV (Fig. 7(b))).

When the reduced inlet velocity is used to simulate the effect of vocal fold closure, we can observe a large vortical structure (Fig. 8(b)) right next to vocal fold which is not present in the case of the model with non-zero leakage (Fig. 8(a)). This flow structure can affect the movement of vocal folds and may play some importance when examining difference between normal and pathological phonation. It is important to stress that the current model is simplified and that the real vocal folds have different shape and can produce different flow structures near vocal folds.

E. Conclusion

Results of 2D and 3D computations of the flow in the vocal chord were presented. Discontinuous Galerkin method was used for spatial discretization of compressible Navier-Stokes equations in ALE formulation. We studied effect of 2D/3D model as well as effect of reduction of inlet velocity on the deflection of glottal jet. We found out that our results are consistent with the hypothesis, that the jet asymmetric deflection

ISBN: 978-988-19253-1-2
ISSN: 2078-0958 (Print); ISSN: 2078-0966 (Online)

(a) Diverging shape of glottis, $-40\,^{\circ}$.

(b) Converging shape of glottis, $40\,^{\circ}$.

Fig. 2. Details of glottis extreme shapes.

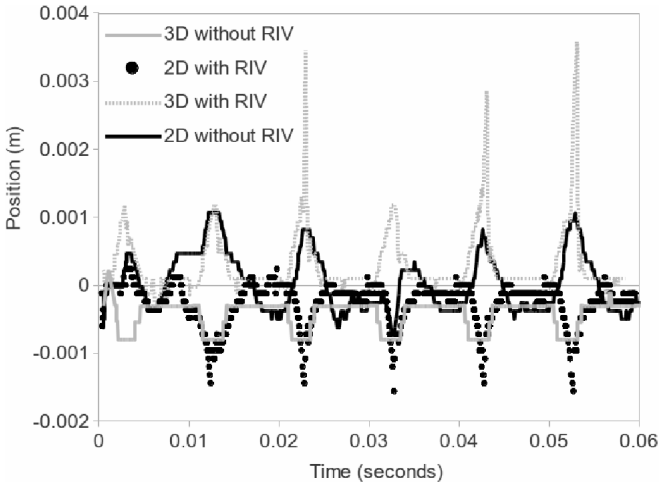

Fig. 9. Y-coordinate of a point with the highest velocity 0.003 cm downstream the glottal folds in six phonation cycles for two 2D and two 3D cases.

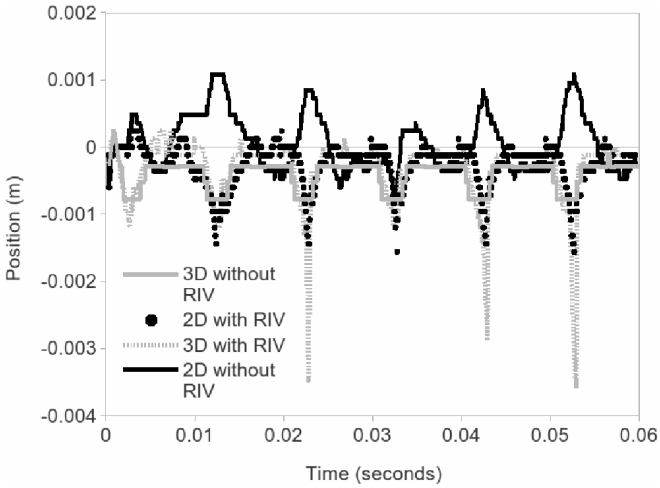

Fig. 10. Y-coordinate of a point with the highest velocity 0.003 cm downstream the glottal folds in six phonation cycles for two 2D and two 3D cases. 3D with RIV line was multiplied by -1 to show the deflection angles.

is result of interaction of the jet and vortices in the postglottal region. Even though the flow structure differs significantly between 2D and 3D flow, the resulting deflection angles are less affected. We also showed importance of modelling the closure of vocal folds to resulting flow structures and to the deflection angles.

REFERENCES

[1] F. Alipour, Ch. Brücker, D.D. Cook, A. Gömmel, M. Kaltenbacher, W. Mattheus, L. Mongeau, E. Nauman, R. Schwarze, I. Tokuda and S. Zörner, "Mathematical Models and Numerical Schemes for Simulation of Human Phonation", *Current Bioinformatics*, vol. 6, pp. 323-343, 2011.

[2] F. Alipour and I.R. Titze, "Combined Simulation of Two-Dimensional Airflow and Vocal Fold Vibration," in *P. J. Davis and N. H. Fletcher (editors): Vocal Fold Physiology, Controlling Complexity and Chaos*, San Diego, 1996.

[3] J. Česenek, M. Feistauer, J. Horáček, V. Kučera and J. Prokopová, "Simulation of Compressible Viscous Flow in Time-Dependent Domains," *Applied Mathematics and Computation*, vol. 219, pp. 7139-7150, 2013.

[4] J. Česenek, M. Feistauer, A. Kosík, "DGFEM for the Analysis of Airfoil Vibrations Induced by Compressible Flow," *ZAMM. Zeitschrift für Angewandte Mathematik und Mechanik. Applied Mathematics and Mechanics*, vol. 93, pp. 387-402, 2013.

[5] V. Dolejší, "Semi-Implicit Interior Penalty Discontinuous Galerkin Methods for Viscous Compressible Flows," *Communications in Computational Physics*, vol. 4, pp. 231-274, 2008.

[6] M. Feistauer, J. Horáček, M. Růžička, P. Sváček, "Numerical Analysis of Flow-Induced Nonlinear Vibrations of an Airfoil with Three Degrees of Freedom," *Computers & Fluids*, vol. 49, pp. 110-127, 2011.

[7] J. Horáček, P. Šidlof and J.G. Švec, "Numerical Simulation of Self-Oscillations of Human Vocal Folds with Hertz Model of Impact Forces," *Journal of Fluids and Structures*, vol. 20, pp. 853-869, 2005.

[8] S. Balay, W. Gropp, and L-C. McInnes. Petsc user manual. http://www.mcs.anl.gov/petsc.

[9] GMSH mesh generator: http://www.geuz.org/gmsh

[10] R. Scherer, D. Shinwari,K.D. Witt,C. Zhang,B. Kucinschi,A. Afjeh, "Intraglottal Pressure Profiles for a Symmetric and Oblique Glottis with a Divergence Angle of $10\,^{\circ}$", *Journal of the Acoustical Society of America*, vol. 109, pp. 1616-1630, 2001.

[11] P. Šidlof, J. Horáček and V. Řídký, "Parallel CFD Simulation of Flow in a 3D Model of Vibrating Human Vocal Folds," *Computers & Fluids*, vol.80, pp. 290-300, 2013.

[12] S. Thomson, J. Tack and G. Verkerke, "A Numerical Study of the Flow-Induced Vibration Characteristics of a Voice Producing Element for Laryngectomized Patient," *Journal of Biomechanics*, vol. 40, pp. 3598-3606, 2007.

[13] I.R. Titze, "Principles of Voice Production," in *National Center for Voice and Speech*, Iowa City, 2000.

[14] I.R. Titze, "The Myoelastic Aerodynamic Theory of Phonation," in *National Center for Voice and Speech, Denver and Iowa City*, 2006.

[15] M.P. De Vries, H.K. Schutte, A.E.P. Veldman and G.J. Verkerke, "Glottal Flow through a Two-Mass Model: Comparison of Navier-Stokes Solutions with Simplified Models," *Journal of the Acoustical Society of America*, vol. 111, pp. 1874-1853, 2002.

[16] X. Zheng and R. Mittal,"A Computational Study of Asymmetric Glottal Jet Deflection during Phonation," *Journal of the Acoustical Society of America*, vol. 129, pp. 2133-2143, Apr. 2011.

ISBN: 978-988-19253-1-2
ISSN: 2078-0958 (Print); ISSN: 2078-0966 (Online)

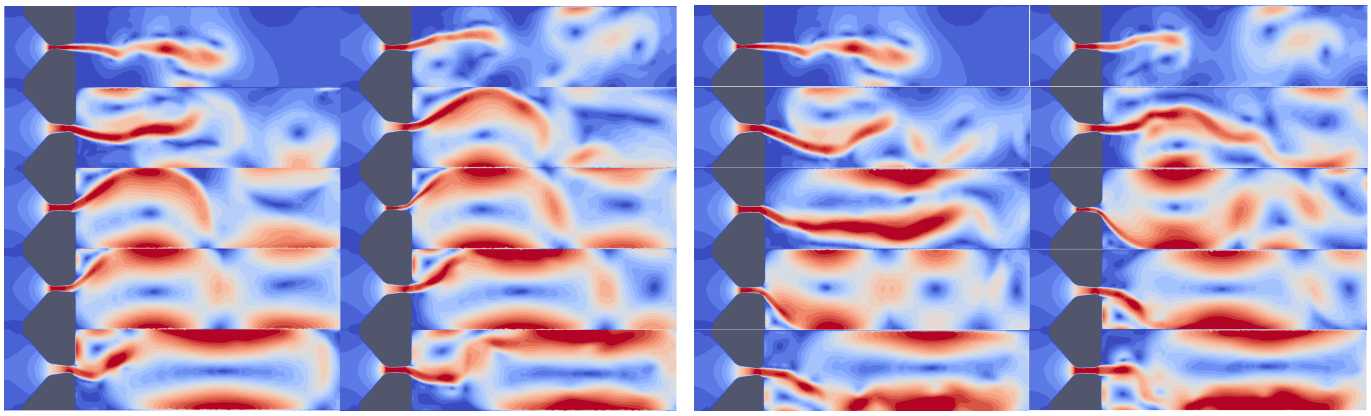

(a) (b)

Fig. 3. Velocity magnitude in different time instants in 2D case, (a) case without reduced inlet velocity, (b) with reduced inlet velocity.

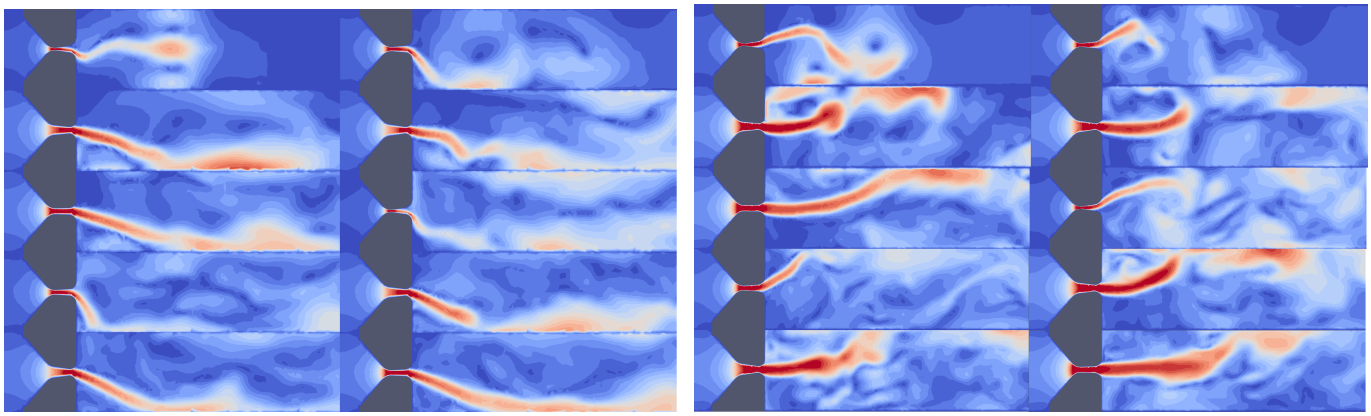

(a) (b)

Fig. 4. Velocity magnitude in different time instants in 3D case, (a) case without reduced inlet velocity, (b) with reduced inlet velocity.

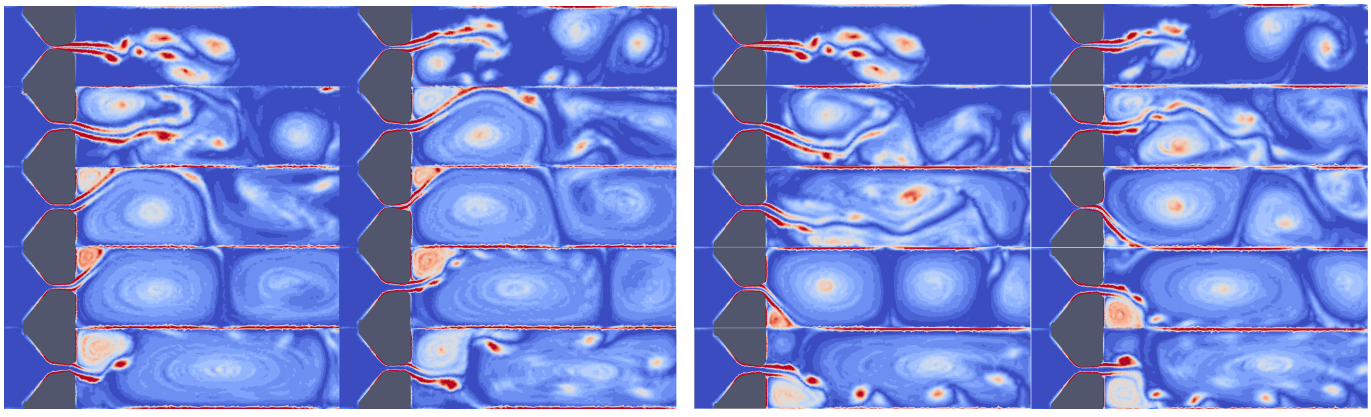

(a) (b)

Fig. 5. Vorcity in 2D case, (a) case without reduced inlet velocity, (b) with reduced inlet velocity.

ISBN: 978-988-19253-1-2
ISSN: 2078-0958 (Print); ISSN: 2078-0966 (Online)

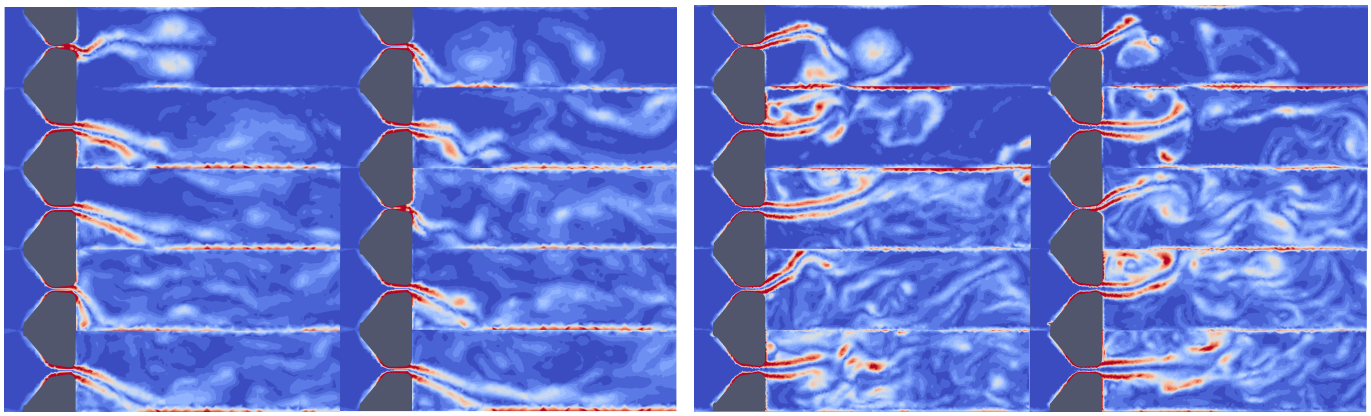

(a) (b)

Fig. 6. Vorcity in 3D case, (a) case without reduced inlet velocity, (b) with reduced inlet velocity.

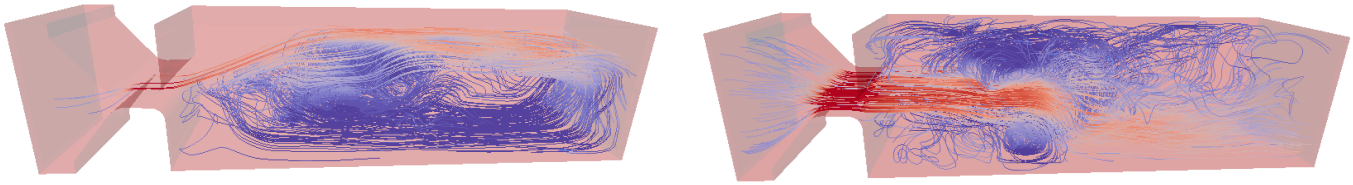

(a) (b)

Fig. 7. Visualization of vortical structures, (a) case without reduced inlet velocity, (b) with reduced inlet velocity.

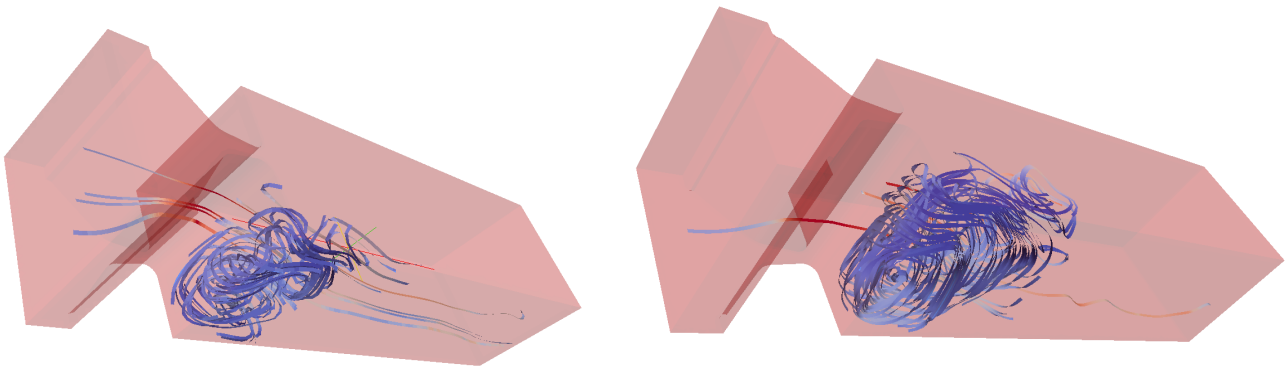

(a) (b)

Fig. 8. Visualization of vortical structure near vocal fold, (a) case without reduced inlet velocity, (b) with reduced inlet velocity.

ISBN: 978-988-19253-1-2
ISSN: 2078-0958 (Print); ISSN: 2078-0966 (Online)